

FAST interstellar scintillation observation of PSR B1929+10 and PSR B1842+14

Ju-Mei Yao^{1,2}, Wei-Wei Zhu¹, Pei Wang¹, Di Li¹, Ji-Guang Lu¹, Fei-Fei Kou¹, Ye-Zhao Yu^{1,3}, Bo Peng¹ and FAST Collaboration¹

¹ CAS Key Laboratory of FAST, National Astronomical Observatories, Chinese Academy of Sciences, Beijing 100101, China; zhuww@nao.cas.cn

² Xinjiang Astronomical Observatories, Chinese Academy of Sciences, Urumqi 830011, China

³ School of Physics and Electronics, Qiannan Normal University for Nationalities, Duyun 558000, China

Received 2019 April 1; accepted 2019 August 16

Abstract In this paper, we present the Five-hundred-meter Aperture Spherical radio Telescope (FAST) observations of PSRs B1929+10 and B1842+14. Through analysis of the pulsars' scintillation pattern, we detected the known scintillation arc from PSR B1929+10 and two previously undetected scintillation arcs from B1842+14. We find that the B1929+10 arc's curvature scales with observing frequency as $\eta_- \propto \nu^{-2.1 \pm 0.1}$ and $\eta_+ \propto \nu^{-1.8 \pm 0.2}$, consistent with Arecibo results and the theoretical expectations of $\eta \propto \nu^{-2}$. From the arc curvature, we infer the scattering screen to be located at 0.20 ± 0.02 kpc from the Earth, close to what was measured by RadioAstron at 324 MHz. From B1842+14, we find two scintillation arcs for the first time. The arcs' curvatures imply that they are caused by two scattering screens located at a distance of 0.3 ± 0.2 kpc and 1.6 ± 0.6 kpc from the Earth, respectively. The screen distance uncertainties mainly come from the uncertainty in pulsar's dispersion measure (DM)-derived distance. We present these FAST scintillation observations and discuss the future prospect of FAST pulsar scintillation study.

Key words: FAST — pulsars: general — ISM: structure

1 INTRODUCTION

Pulsar interstellar scintillation refers to the flickering of pulsar brightness that arises from the relative motion between the pulsar, the inhomogeneous interstellar medium and the Earth (Rickett 1990). Pulsar scintillation observations are a powerful tool for studying both pulsars and the turbulent ionized interstellar medium along different line of sights. Using dynamic spectrum – the pattern of pulsar brightness variation in both time and frequency – we can measure the scintillation parameters and then study their frequency dependence to verify different theories of turbulence (Wang et al. 2005). The squared modulus of the two-dimensional Fourier transform of a dynamic spectrum is the secondary spectrum. In the secondary spectra, Stinebring et al. (2001) first discovered parabolic arcs and, subsequently parabolic arcs with inverted arclets, multiple parabolic arcs and asymmetric parabolic arcs were detected from some pulsars (see Heiles & Stinebring 2007; Trang

& Rickett 2007; Brisken et al. 2010). From arcs and arclets we can measure the scale, location and velocity of the scattering medium and velocity of the pulsar. For pulsars in binary systems, the variation of scintillation timescale and arc curvature may enable us to constrain the binary orbit (Lyne 1984; Ord et al. 2002; Reardon et al. 2019). For some pulsar-timing array (PTA) pulsars, scintillation observations may help us understand the influence of the interstellar medium on pulsar timing accuracy (Hemberger & Stinebring 2008). To date, parabolic arcs have been detected for 32 pulsars of which only two are in binary systems (e.g., Stinebring et al. 2001; Putney et al. 2005; Kerr et al. 2018; Fadeev et al. 2018; Wang et al. 2018). When the scintillation timescale and bandwidth are resolvable, the detectability of arcs mainly relies on the telescope's sensitivity (Xu et al. 2018), where the Five-hundred-meter Aperture Spherical radio Telescope (FAST) has significantly comparative strength. According to Jiang et al. (2019), in L -band FAST's sensitivity is about 2 and 9 times higher than

Arecibo Observatory and Green Bank Telescope, respectively. Therefore, FAST will likely be able to detect arcs for more pulsars. These scintillation arcs may enable us to study the boundary of the local hot bubble, the Galactic spiral arms, or the orbit of some binary systems.

In this paper, we conducted interstellar scintillation analysis for FAST observation of PSR B1929+10 and PSR B1842+14. Both pulsars are located in the visible sky of the Arecibo telescope. PSR B1929+10 is the brighter of the two with mean flux density of 28.7 mJy at 1400 MHz, and its scintillation arc was found by Hill et al. (2003) using Arecibo observation. PSR B1842+14 is dimmer ($S_{1400} = 1.8$ mJy) and no scintillation arc was found from it using the Arecibo telescope. We observed these two pulsars using 30 min long FAST tracking and detected scintillation arcs from both of them.

The arrangement of our paper is as follows. We describe the observation and the data processing procedures in Section 2. In Section 3 and Section 4, we show the interstellar scintillation results for PSR B1929+10 and PSR B1842+14, respectively, and then summarize our discussion and main conclusions in Section 5.

2 OBSERVATIONS AND DATA PROCESSING

We carried out the scintillation observations of PSRs B1929+10 and B1842+14 using the FAST radio telescope’s 19-beam receiver in L -band. The 19-beam receiver collects detected filterbank data with two polarizations, the data were sampled at 49.152 μ s intervals and with 4096 channels of 0.122 MHz width between 1000 and 1500 MHz. The top and the bottom 50 MHz are not in the designed band of the receiver. Therefore, we only use data in a total effective bandwidth of 400 MHz between 1050 and 1450 MHz. We conducted 30 min tracking observations for PSRs B1929+10 and B1842+14. We used PSRCHIVE software package (van Straten et al. 2012)¹ to reduce our data. We folded the data for each channel with a sub-integration time of $\delta t = 10$ s and then summed the two polarizations to form total pulse intensity. We removed the RFI in frequency channels and sub-integrations and replaced it with adjacent intensity value using the *pazi* command, and then formed the dynamic spectrum using the *psrflux* command. Since we used a channel bandwidth of $\Delta\nu = 0.122$ MHz and an integration time of $\Delta t = 10$ s, the corresponding Nyquist frequencies in our secondary spectrum were $f_t(\text{Nyquist}) = 50$ mHz and $f_\nu(\text{Nyquist}) = 4.1$ μ s. Following Stinebring et al. (2019), we described the parabolic arc in the secondary spectrum

as

$$f_\nu = \eta f_t^2, \quad (1)$$

and define the arc curvature as

$$\eta = 0.4625 \times 10^4 \frac{D_{\text{kpc}}}{\nu_{\text{GHz}}^2 (V_{\text{eff},\perp} \cos\psi)^2} s(1-s) \text{ s}^3, \quad (2)$$

where D is pulsar distance in kpc, ν is observing frequency in GHz, s is the relative distance of the scattering screen to the pulsar, $V_{\text{eff},\perp}$ is the effective perpendicular velocity in km s^{-1} and ψ is the angle between the major axis of the anisotropic structure and the effective velocity vector. According to Cordes & Rickett (1998), the $V_{\text{eff},\perp}$ comes from three components:

$$V_{\text{eff},\perp} = (1-s)V_{\text{psr},\perp} + sV_{\text{Earth},\perp} - V_{\text{scr},\perp}, \quad (3)$$

where $V_{\text{psr},\perp}$, $V_{\text{Earth},\perp}$ and $V_{\text{scr},\perp}$ are transverse velocity of pulsar, Earth and scattering medium respectively. We could calculate the relative distance of the scattering screen s using our measured arc curvature η by assuming medium transverse velocity to be negligible and $\psi = 0$. Following this, we can derive the distance of the scattering screen to the Earth to be $D_{\text{kpc}}(1-s)$ in kpc.

3 INTERSTELLAR SCINTILLATION RESULTS OF PSR B1929+10

For PSR B1929+10, we conducted the 30 min observations on 2018 September 21. The 30 min dynamic spectrum was not able to cover one complete scintillation scintle as in L -band the scintillation timescale is larger than 30 min. This is consistent with the previous scintillation timescale of 32 min measured by Wang et al. (2005) at 1540 MHz using 6-h observations of the Nanshan 25-m telescope.

3.1 Secondary Spectrum and Frequency Dependence of Arc Curvature

Through multifrequency observations of PSRs B0834+06, B1133+16 and B1929+10 at Arecibo Observatory, Hill et al. (2003) found that the frequency dependence of arc curvatures is consistent with the theoretical predictions by the simple thin scattering screen geometry ($\eta \propto \nu^{-2}$).

To analyze the frequency dependence of arc curvature from B1929+10 as measured by FAST, we divided our 400 MHz bandwidth into four equal subbands of 100 MHz wide. The center frequencies of the subbands are 1100, 1200, 1300 and 1400 MHz, respectively. Figure 1 showed the corresponding secondary spectra at four frequencies with frequency increasing from the top to the bottom panels, and the arc curvature decreased obviously with the increasing of the frequency. Because the scintillation arcs

¹ <http://psrchive.sourceforge.net>

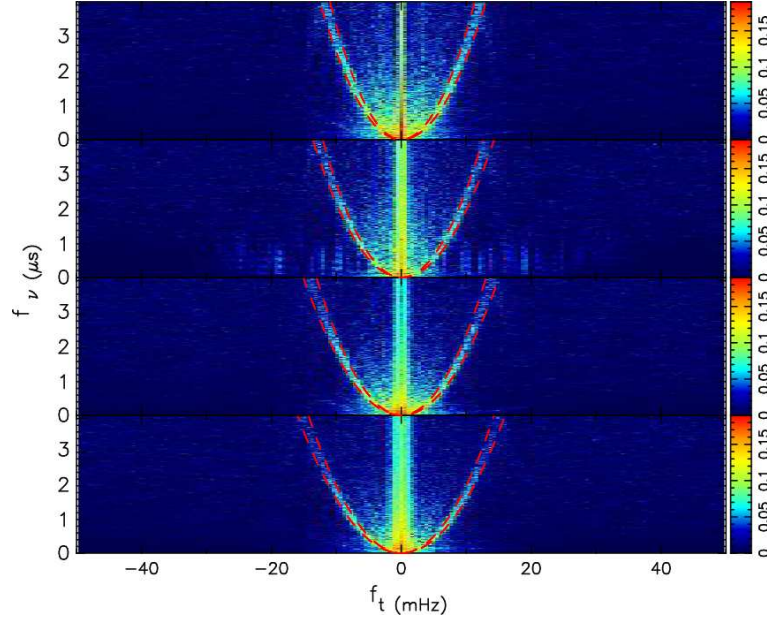


Fig. 1 The secondary spectra of PSR B1929+10 from four subbands. From top to bottom, the subband center frequencies are 1100, 1200, 1300, and 1400 MHz, respectively. The horizontal and vertical axes are conjugate time (f_t) and conjugate frequency (f_ν). The red dashed lines show the boundaries of the scintillation arcs.

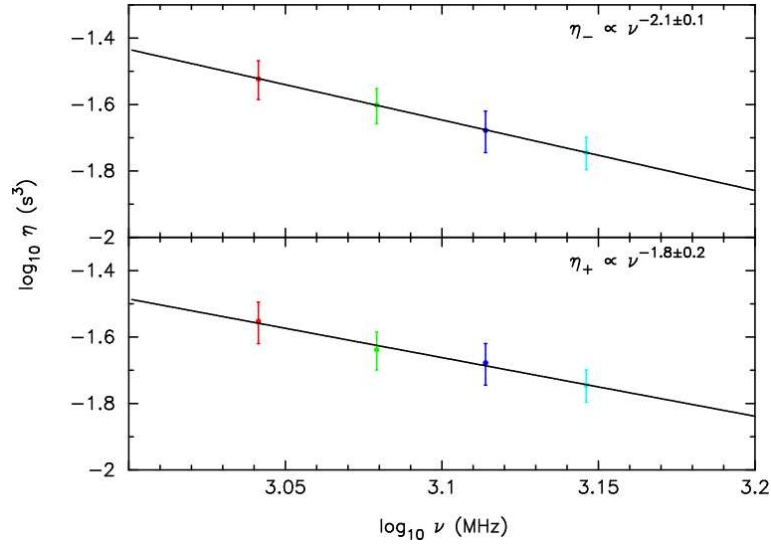


Fig. 2 The frequency dependence of arc curvature at negative and positive f_t for PSR B1929+10. Arc curvatures centered at 1100, 1200, 1300, and 1400 MHz are plotted as red, green, blue and cyan points, respectively.

were not completely axisymmetric with the central f_ν axis, we chose to quantify the arc curvatures on both negative f_t and positive f_t regions. To measure the arc curvature, we overplotted parabolas on the secondary spectra with different curvature parameters and decided the best fit to the parabolic arc by eye, and uncertainties were calculated by fitting the parabolas to the boundary of each parabolic arc. In Figure 2, arc curvatures with uncertainties were plotted as a function of observing frequency on log-log plot for

both negative f_t and positive f_t , respectively, and the data fitting resulted in $\eta_- \propto \nu^{-2.1 \pm 0.1}$ and $\eta_+ \propto \nu^{-1.8 \pm 0.2}$. We traced out the boundaries of the scintillation arcs by eye to estimate arc curvature uncertainties, and this method tended to overestimate the uncertainties. Indeed, the error bars of arc curvatures seemed slightly bigger than the scatter of the points in Figure 2. We tentatively conclude that the arc curvatures appeared to follow the expected relation-

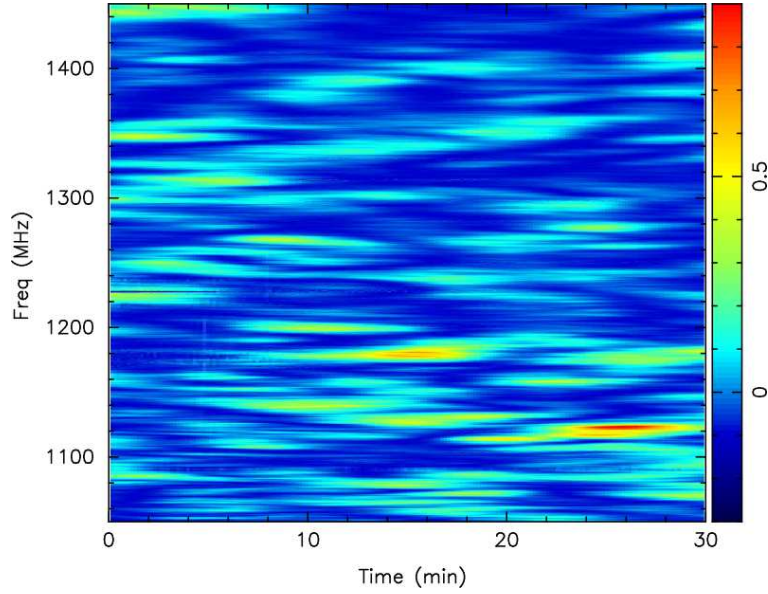


Fig. 3 The dynamic spectrum for the 30 min observation of B1842+14 taken on 2018 August 28. The horizontal and vertical axes correspond to the time and frequency, respectively.

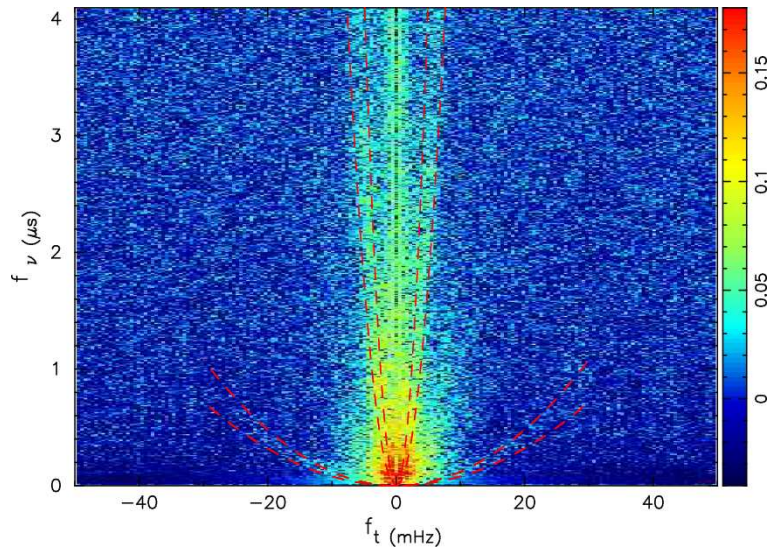


Fig. 4 The secondary spectrum of B1842+14 at 1400 MHz. The horizontal and vertical axes are conjugate time (f_t) and conjugate frequency (f_ν). The *red dashed lines* show the boundaries of the scintillation arcs.

ship with frequency (Hill et al. 2003), noting the caveats in our current method.

According to VLBI observations, PSR B1929+10 is located at 0.36 ± 0.01 kpc from the Earth and the transverse velocity in right ascension and declination are 161 ± 5 km s⁻¹ and 74 ± 2 km s⁻¹, respectively (Kirsten et al. 2015). We considered Earth velocity in the calculation of the scattering screen location, because of its remarkable effect on arc curvature (Stinebring et al. 2005). We calculated the Earth’s relative velocity to PSR B1929+10 are 11 km s⁻¹ and 16 km s⁻¹ in the directions of right ascen-

sion and declination, using the CALCEPH software package (Gastineau et al. 2015)². We derived that the relative position of the screen s is 0.434 ± 0.031 by using the best-measured arc curvature of $\eta = 0.018 \pm 0.002$ s³ from the top band centered at 1400 MHz (Eq. (2)). Then we found the corresponding scattering screen located at 0.20 ± 0.02 kpc from the Earth, consistent with the value of 0.24 ± 0.03 kpc measured by RadioAstron observations at 324 MHz (Fadeev et al. 2018).

² <https://www.imcce.fr/inpop/calceph/>

4 INTERSTELLAR SCINTILLATION RESULTS OF PSR B1842+14

In the following subsection, we show the scintillation analysis for the 30 min observations of PSR B1842+14 taken on 2018 August 28.

4.1 Dynamic Spectrum and Secondary Spectrum

In Figure 3, we showed the dynamic spectrum of PSR B1842+14 with total frequency bandwidth of 400 MHz. From the dynamic spectra in Figure 3, both the scintillation bandwidth and scintillation timescale were resolvable and the scale of the scintillation scintles gradually increased with increasing of the central frequency. We found two scintillation arcs in secondary spectra. The inner arc had especially large curvature and arc curvature decreased with observing frequency, so we chose to show only the corresponding secondary spectrum at 1400 MHz in Figure 4. By using the same method for PSR B1929+10, we found that the curvature of the inner and outer arcs are $\eta_{\text{inner}} = 0.12 \pm 0.05 \text{ s}^3$ and $\eta_{\text{outer}} = 0.0010 \pm 0.0002 \text{ s}^3$, respectively. Yao et al. (2017) estimated that about 68% of the DM-distances given by their model have relative uncertainty of less than 40%. We took 40% uncertainties as a rough one-sigma error for the DM-distance of PSR B1842+14, i.e., $D = 1.7 \pm 0.7 \text{ kpc}$. Harrison et al. (1993) measured the total proper motion of PSR B1842+14 to be $46 \pm 6 \text{ mas yr}^{-1}$, and the transverse velocity $V_{\text{psr},\perp} = 366 \pm 190 \text{ km s}^{-1}$. We did not consider the Earth’s motion because it is negligible when compared with pulsar’s transverse velocity and its uncertainty, coming largely from the poorly constrained pulsar distance. From Equation (2), we estimated $s_{\text{inner}} = 0.80 \pm 0.05$ and $s_{\text{outer}} = 0.033 \pm 0.006$. Therefore, the scattering screen causing the inner arc is located at $0.3 \pm 0.2 \text{ kpc}$ from the Earth, and the outer-arc screen is located at $1.6 \pm 0.6 \text{ kpc}$ from the Earth. The uncertainties in these distances are mainly attributed to the uncertainty in the pulsar’s DM-derived distance, so independent distance measurement would be vital for obtaining more accurate scattering screen locations. With a mean flux density of 1.8 mJy at 1400 MHz, PSR B1842+14 is dimmer than the dimmest pulsar (PSR B1737+13, $S_{1400} = 2.1 \text{ mJy}$) with scintillation arcs detected by Arecibo in *L*-band. Using B1842+14 as a reference, we speculated that pulsars with mean flux density divided by duty cycle (i.e., peak flux density: S_{peak}) higher than 8 mJy, and a decent amount of transverse velocity could possibly produce detectable scintillation arcs.

5 DISCUSSION AND CONCLUSIONS

Using FAST’s observation in the commissioning phase, we detected scintillation arcs for PSR B1929+10 and B1842+14. Among the 32 pulsars with scintillation arc detection, PSR B1929+10 is one of the closest bright low-DM pulsars. Its narrow arc structure makes it an ideal target for studying frequency dependence of arc curvature. Within FAST’s 19-beam receiver bandwidth, we find that the arc curvatures in negative f_t and positive f_t regions scale with observing frequency as $\eta_- \propto \nu^{-2.1 \pm 0.1}$ and $\eta_+ \propto \nu^{-1.8 \pm 0.2}$, which are consistent with the previous Arecibo result ($\eta \propto \nu^{-2.1 \pm 0.1}$) and theoretical predictions by a simple thin scattering screen model (Hill et al. 2003). The FAST *L*-band constraint on η ’s frequency dependency is very close to that of Arecibo, despite the fact that the Arecibo result was achieved with multi-band observations of longer integration. We also measured a consistent scattering screen distance of $0.20 \pm 0.02 \text{ kpc}$ from the Earth. Using 30 min FAST observations, we detected the scintillation arcs from B1842+14 for the first time. The two arcs enabled us to derive the locations of scattering screens of $0.3 \pm 0.2 \text{ kpc}$ and $1.6 \pm 0.6 \text{ kpc}$ from the Earth.

Thanks to its superior sensitivity and larger sky coverage than the Arecibo telescope, the FAST would likely be able to detect new scintillation arcs from many pulsars. We estimated that the scintillation bandwidth for pulsars with $\text{DM} \sim 70 \text{ pc cm}^{-3}$ is comparable to the frequency resolution of FAST in its 19 beam band. Scintillation analysis for pulsars with $\text{DM} > 70 \text{ pc cm}^{-3}$ would require smaller channel bandwidth than FAST currently provides (0.125 MHz), or higher observing frequency (Wang et al. 2018). By using B1842+14 as a reference, excluding pulsars with $\text{DM} > 70 \text{ pc cm}^{-3}$ and pulsars with scintillation timescale longer than 30 min, we still found more than 20 pulsars from which FAST could detect new scintillation arcs. Detecting arcs, arclets and other secondary spectrum structures from these pulsars will enable us to study the Galactic interstellar medium structures with more details in the near future.

Acknowledgements We thank the referee for helpful comments that have resulted in significant improvements to the paper. This work was supported by the CAS “Light of West China” Program 2017-XBQNXZ-B-022, the “Tianchi Doctoral Program 2017”, the CAS International Partnership Program (No. 114A11KYSB20160008), the Strategic Priority Research Program of the Chinese Academy of Sciences (Grant No. XDB23000000). This project was also supported by the National Natural Science Foundation of China (Grant Nos. 61472043, 11743002,

11873067, 11690024, 11725313 and U1831104). WWZ is supported by the Chinese Academy of Science Pioneer Hundred Talents Program. The FAST fellowship was supported by Special Funding for Advanced Users, budgeted and administrated by Center for Astronomical Mega-Science, Chinese Academy of Sciences (CAMS).

References

- Brisken, W. F., Macquart, J.-P., Gao, J. J., et al. 2010, *ApJ*, 708, 232
- Cordes, J. M., & Rickett, B. J. 1998, *ApJ*, 507, 846
- Fadeev, E. N., Andrianov, A. S., Burgin, M. S., et al. 2018, *MNRAS*, 480, 4199
- Gastineau, M., Laskar, J., Manche, H., & Fienga, A. 2015, CALCEPH: Planetary Ephemeris Files Access Code, Astrophysics Source Code Library, ascl:1505.001
- Harrison, P. A., Lyne, A. G., & Anderson, B. 1993, *MNRAS*, 261, 113
- Heiles, C., & Stinebring, D. 2007, astro-ph/0701656
- Hemberger, D. A., & Stinebring, D. R. 2008, *ApJ*, 674, L37
- Hill, A. S., Stinebring, D. R., Barnor, H. A., Berwick, D. E., & Webber, A. B. 2003, *ApJ*, 599, 457
- Jiang, P., Peng, B., Li, D., & Xu, R. 2019, arXiv:1903.07240
- Kerr, M., Coles, W. A., Ward, C. A., et al. 2018, *MNRAS*, 474, 4637
- Kirsten, F., Vlemmings, W., Campbell, R. M., Kramer, M., & Chatterjee, S. 2015, *A&A*, 577, A111
- Lyne, A. G. 1984, *Nature*, 310, 300
- Ord, S. M., Bailes, M., & van Straten, W. 2002, *ApJ*, 574, L75
- Putney, M. L., Minter, A. H., Stinebring, D. R., & Ransom, S. M. 2005, in *Bulletin of the American Astronomical Society*, 37, American Astronomical Society Meeting Abstracts, 1470
- Reardon, D. J., Coles, W. A., Hobbs, G., et al. 2019, *MNRAS*, 485, 4389
- Rickett, B. J. 1990, *ARA&A*, 28, 561
- Stinebring, D. R., Hill, A. S., & Ransom, S. M. 2005, in *Astronomical Society of the Pacific Conference Series*, 328, Binary Radio Pulsars, eds. F. A. Rasio, & I. H. Stairs, 349
- Stinebring, D. R., McLaughlin, M. A., Cordes, J. M., et al. 2001, *ApJ*, 549, L97
- Stinebring, D. R., Rickett, B. J., & Koch Ocker, S. 2019, *ApJ*, 870, 82
- Trang, F. S., & Rickett, B. J. 2007, *ApJ*, 661, 1064
- van Straten, W., Demorest, P., & Osłowski, S. 2012, *Astronomical Research and Technology*, 9, 237
- Wang, N., Manchester, R. N., Johnston, S., et al. 2005, *MNRAS*, 358, 270
- Wang, P. F., Han, J. L., Han, L., et al. 2018, *A&A*, 618, A186
- Xu, Y. H., Lee, K. J., Hao, L. F., et al. 2018, *MNRAS*, 476, 5579
- Yao, J. M., Manchester, R. N., & Wang, N. 2017, *ApJ*, 835, 29